

Structural, magnetic, thermodynamic and electrical transport properties of a new compound $\text{Pr}_2\text{Rh}_2\text{Ga}$

Baidyanath Sahu,^{1, a)} Sindisiwe P. Xhakaza,¹ and André M. Strydom¹

Highly Correlated Matter Research Group, Physics Department, University of Johannesburg, PO Box 524, Auckland Park 2006, South Africa

A new ternary intermetallic compound $\text{Pr}_2\text{Rh}_2\text{Ga}$ was synthesized by arc-melting and was characterized by powder X-ray diffraction (PXRD), magnetization, heat capacity $C_p(T)$, and electrical resistivity $\rho(T)$ measurements. PXRD patterns revealed that $\text{Pr}_2\text{Rh}_2\text{Ga}$ crystallizes in the La_2Ni_3 -type of orthorhombic structure with the space group $Cmca$. The temperature variation of magnetic susceptibility, $C_p(T)$ and $\rho(T)$ confirmed that $\text{Pr}_2\text{Rh}_2\text{Ga}$ exhibits a ferromagnetic behavior with the transition temperature of 18 K. The estimated Sommerfeld coefficient $\gamma = 640 \text{ mJ}/(\text{Pr.mole.K}^2)$ from the $C_p(T)$ results in the paramagnetic region just above T_C was large in comparison to ordinary metals. In the paramagnetic region of $\rho(T)$ data showed a metallic behavior characteristic of electron - phonon scattering. The maximum negative magneto-resistance at high field occurs in the region near the magnetic phase transition temperature. The maximum value of magnetic entropy change ($-\Delta S_M$) and adiabatic temperature change (ΔT_{ad}) are 8.2 J/kg.K and 3.6 K, respectively, around the transition temperature for the change of magnetic field 0–9 T. The calculated refrigerant capacity is 70 J/kg, and 135 J/kg for a change of magnetic field 0–5 T and 0–9 T, respectively. Arrott plot derived from isothermal magnetization and the universal scaling plot by normalizing $-\Delta S_M$ confirm that the compound undergoes a second order ferromagnetic to paramagnetic phase transition.

Keywords: Ferromagnet; Spin wave; Heat capacity; Electrical resistivity; Magnetoresistance; Magnetocaloric

A. Introduction

The Praseodymium (Pr) based ternary compounds present interesting magnetic, electric and thermal transport properties such as non-magnetic ordering, ferro and antiferromagnetic behavior, heavy fermion^{1–6}, Kondo behavior⁷ and superconductivity⁸. The magnetic and transport properties of Pr-compounds are strongly influenced by the crystal electric field (CEF). Pr-based ternary compounds are also attractive for the heavy fermion superconductivity properties. Bauer *et. al.*⁸, observed the occurrence of a heavy-fermion superconductivity state in the $\text{PrOs}_2\text{Pb}_{12}$ compound. Similarly, Zhang *et. al.*⁹, have reported multiband superconductivity in $\text{PrPt}_2\text{Ge}_{12}$ compound with critical temperature of 8 K. Additionally, Pr-compounds such as PrCu_2In^2 , $\text{PrCo}_2\text{B}_2\text{C}^{10}$, and $\text{PrNi}_2\text{B}_2\text{C}^{11}$ show large Sommerfeld coefficient values.

Recently $\text{RE}_2\text{T}_2\text{X}$ (RE = rare earth metal, T = transitions metal and X = p-block elements) series of compounds are of interest for attractive structural and physical properties. $\text{RE}_2\text{T}_2\text{X}$ compounds are known to form in a small number different structure type, which depends on the composition. Most of $\text{RE}_2\text{T}_2\text{X}$ compounds crystallize in Mo_2FeB_2 – type of tetragonal structure with space group $P_4/m\bar{b}m^{12–14}$. A small number of compounds form a superstructure of Mo_2FeB_2 and crystallize in $\text{U}_2\text{Pt}_2\text{Sn}$ -type of tetragonal structure¹⁵. Some of the compounds crystallize in W_2CoB_2 and $\text{Mn}_2\text{B}_2\text{Al}$ – type of orthorhombic structure with space group $Immm$ and $Cmmm$, respectively^{12–14}. Some $\text{RE}_2\text{T}_2\text{X}$ com-

pounds show structural transformation, which depends on the rare-earth size, external pressure and also on processed temperature. For example, a tetragonal to orthorhombic is found in $\text{RE}_2\text{Ni}_2\text{Sn}$ compounds by varying rare-earth elements and external pressure on a particular sample. $\text{Pr}_2\text{T}_2\text{X}$ (T = Cu, Ni and Pd, X = In, Sn) crystallize in the tetragonal Mo_2FeB_2 – type structure^{4,12,16,17}. $\text{Pr}_2\text{Ni}_2\text{Ga}$, $\text{Pr}_2\text{Ni}_2\text{Al}$ and $\text{Pr}_2\text{Co}_2\text{Al}$ crystallize in W_2CoB_2 – type of orthorhombic structure with space group $Immm$. $\text{Pr}_2\text{Co}_2\text{Al}$ shows a structural transformation from orthorhombic to monoclinic at higher temperatures^{18,19}.

Very recently, a new variant of the 2:2:1 formula type was reported, namely $\text{Ce}_2\text{Rh}_2\text{Ga}$ which crystallizes in monoclinic (space group $C2/c$) for without annealing and shows an ordered version of the orthorhombic La_2Ni_3 – structure type with space group $Cmca$ (no-64) for annealing at higher temperature. Surprisingly, this orthorhombic compound was found to exhibit a phase transition at ≈ 125 K that is unusually high among Ce compounds²⁰. In this paper, we have investigated whether other rare-earth elements are amenable to the new 2:2:1 type structure, and report on the synthesis, structure, and physical properties of a new compound $\text{Pr}_2\text{Rh}_2\text{Ga}$. The magnetocaloric effect (MCE) of this compound has also been studied from isothermal magnetization and heat capacity measurements.

B. Experimental detail

A stoichiometric mixture of the elements Pr (99.85 wt.% purity) Rh (99.85 wt.% purity), and Ga (99.999 wt.% purity) with the ratio Pr:Rh:Ga = 2:2:1 and total mass of 1 g for this compound was arc-melted on a water-

^{a)}Corresponding author

cooled copper hearth using an Edmund Bühler GmbH MAM-1 commercial arc furnace. The sample was melted under high purity argon (Ar) atmosphere, where the gas bottle was connected to a Monotorr high-temperature gas getterer. The sample was melted several times to ensure homogeneity. The weight losses after the melting process were confirmed to be less than 1.0 wt. %. The as-cast sample was wrapped in tantalum foil and annealed for one week at 1073 K in an evacuated silica ampoule. Finally the sample was quenched in cold water.

In order to study the phase purity of the annealed sample $\text{Pr}_2\text{Rh}_2\text{Ga}$ was characterized by powder X-ray diffraction (PXRD) using a Rigaku diffractometer with $\text{Cu-K}\alpha$ radiation. Magnetic, heat capacity (C_P) and electrical transport (ρ) properties measurements were performed on a Quantum Design commercial Dynacool, Physical Property Measurement System (PPMS) in the temperature range of 1.8 - 300 K, with applied magnetic field up to 9 T. Heat capacity was measured by employing the two- τ relaxation method. The sample is stacked and thermally coupled to the sample platform using Apiezon N grease. Electrical resistivity measurements were performed by a standard four probe contact method and using an ac-current excitation.

C. Results and Discussions

1. X-ray diffraction

Fig. 1a depicts PXRD pattern measured at room temperature. For investigating the crystal structure and phase purity, the data was processed with a Rietveld refinement method using the FULLPROF software^{21,22}. The PXRD pattern of $\text{Pr}_2\text{Rh}_2\text{Ga}$ along with the refinement fitting is shown in Fig. 1a. The refinement results revealed that this compound crystallizes in the La_2Ni_3 -type of orthorhombic structure belonging to the $Cmca$ space group. In the structure of La_2Ni_3 , the rare-earth atom Pr occupies La site, whereas Rh and Ga occupy the two sites of $\text{Ni}^{20,23}$. The obtained refinement parameters are listed in Table I. A schematic diagram for the crystal structure was generated from the refinement data by using VESTA software and is shown in Fig. 1b²⁴. The details arrangement of atoms in crystal structure is described for the similar compound of $\text{Ce}_2\text{Rh}_2\text{Ga}^{20}$.

The obtained Pr-Pr distances are ranging from 3.431 to 3.710 Å, which is approximately twice the metallic radius of Pr element ($r_{\text{Pr}} = 1.810$ Å)²⁵. The short interatomic distances of Pr-Rh is 2.978 Å, Pr-Ga is 3.334 Å and Rh-Ga is 2.547 Å, which is significantly smaller than the sum of the metallic radius ($r_{\text{Rh}} = 1.345$ Å) and Ga ($r_{\text{Ga}} = 1.411$ Å)²⁵ of two atoms. These results suggest that there is a strong bonding between these elements.

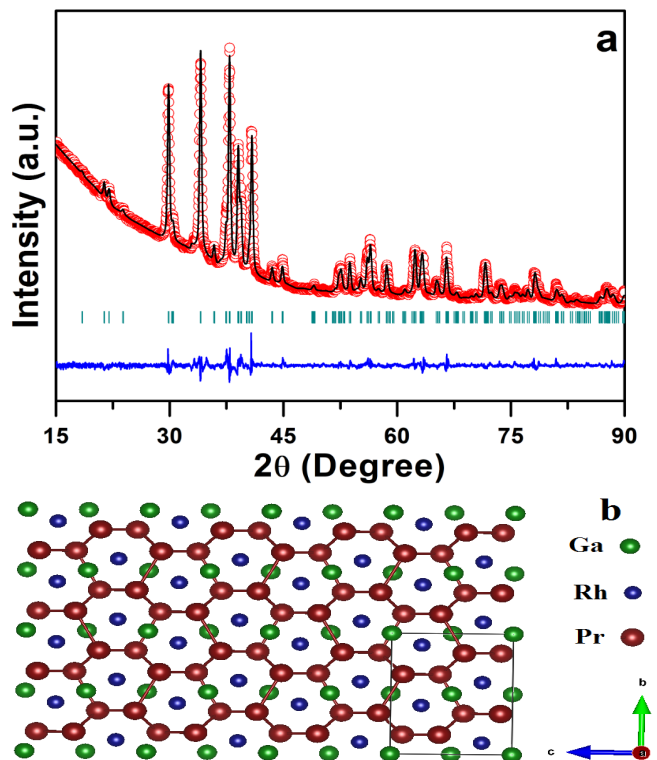


FIG. 1. (a) PXRD patterns along with the Rietveld refinement profile for $\text{Pr}_2\text{Rh}_2\text{Ga}$. The red open circles represent the experimental data and black solid line stands for the calculated pattern from the model structure used in the Rietveld refinement to fit the experimental data. The difference curve is shown as a blue line and the allowed Bragg peaks as vertical bars. (b) Schematic diagram for the crystal structure of $\text{Pr}_2\text{Rh}_2\text{Ga}$.

2. Magnetic properties

The temperature variation of dc-magnetization ($M(T)$) was carried out in both zero field cooled (ZFC) and field cooled (FC) protocol in the applied external magnetic fields of 0.2 T and 0.5 T. In the ZFC process, the sample was cooled down to 2 K in zero field. Thereafter, a field was applied and data were recorded while warming the sample to high temperature. In FC process, the sample was cooled down in presence of magnetic field to 2 K, thereafter data was recorded upon warming from 2 K. Fig. 2 shows the temperature dependence of dc-magnetic susceptibility $\chi(T) = M(T)/H$, for $\text{Pr}_2\text{Rh}_2\text{Ga}$. $\chi(T)$ shows that the sample exhibits ferromagnetic behavior. The Curie temperature T_C was estimated from the peak of the $dM(T)/dT$ of the FC magnetization curve for 0.5 T, and was found to be $T_C = 18$ K, which is shown in inset (a) of Fig. 2. The ferromagnetic transition temperature deduced for $\text{Pr}_2\text{Rh}_2\text{Ga}$ is higher than the reported for $\text{Ce}_2\text{Rh}_2\text{Ga}^{20}$. It is also noteworthy that the ZFC and FC curves start to diverge below T_C , which is known as irreversibility behavior. The

TABLE I. The lattice parameters and unit cell volume $\text{Pr}_2\text{Rh}_2\text{Ga}$ compound obtained from the Rietveld refinements of XRD patterns for Orthorhombic phase along with the atomic coordinate positions.

a		5.869(3) Å		
b		9.607(2) Å		
c		7.464(2) Å		
V		420.80(3) Å ³		
Atomic coordinates for $\text{Pr}_2\text{Rh}_2\text{Ga}$				
Atom	Wyckoff	x	y	z
Pr	8f	0	0.3385(2)	0.0981(2)
Rh	8e	1/4	0.0961(1)	1/4
Ga	4a	0.0	0.0	0.0

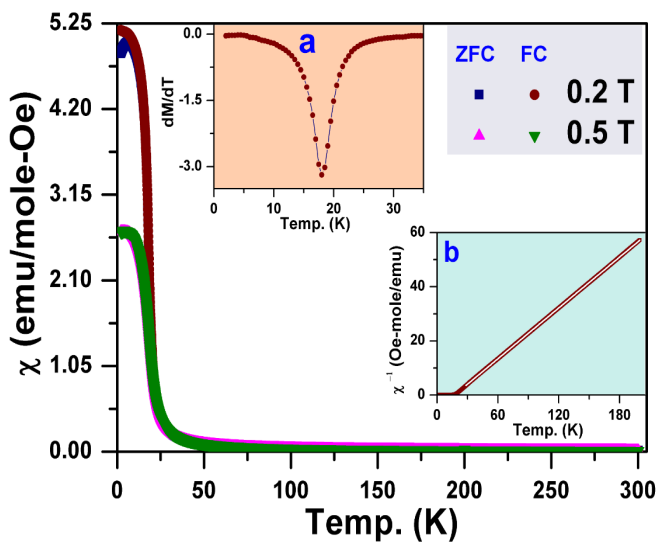


FIG. 2. Temperature dependence of the dc-magnetic susceptibility $\chi(T)$ of $\text{Pr}_2\text{Rh}_2\text{Ga}$ in the field-cooled (FC) and zero-field-cooled (ZFC) process. Inset (a) shows the $dM(T)/dT$ of FC curve under 0.2 T to estimate the transition temperature. Inset (b) temperature variation inverse magnetic susceptibility of FC curve under 0.2 T.

difference between ZFC and FC magnetization becomes negligible for the applied field of 0.5 T. This irreversibility behavior at small value of applied magnetic field probably arises due to the presence of uniaxial anisotropy associated with 4f-electron cations, short-range magnetic ordering or the domain wall pinning effect²⁶. However, in this case, the ZFC magnetization decreases with decrease in temperature far below T_C , which causes the irreversibility behavior. This point towards domain wall pinning due to the magnetocrystalline anisotropy of the Pr^{3+} ions, as a probable cause of the irreversibility behavior in the compound⁶.

The temperature variation of inverse dc-magnetic susceptibility, $\chi^{-1}(T)$ for $H = 0.2$ T is depicted in inset (b)

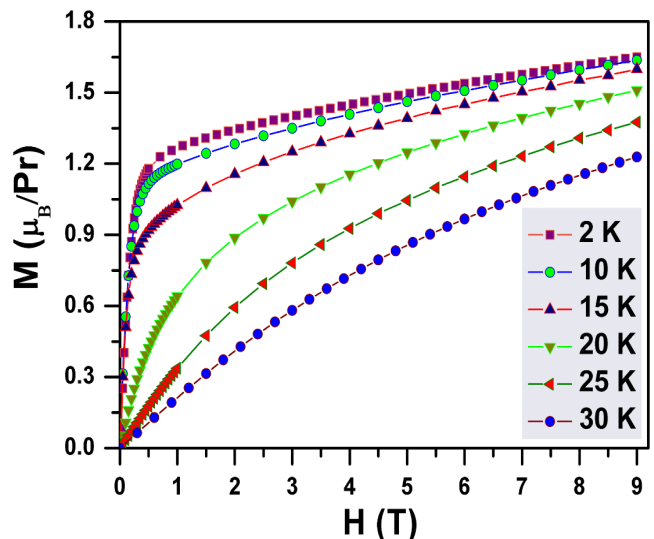


FIG. 3. Isothermal magnetization at different temperatures.

of Fig. 2. The $\chi^{-1}(T)$ graph shows a linear behavior at temperatures above 20 K, which follows the Curie–Weiss law; $\chi(T) = C/(T - \theta_p)$, where C is the Curie constant and is defined as $C = N\mu_{\text{eff}}^2/3k_B$. θ_p is the paramagnetic Weiss temperature. A linear fit to the inverse susceptibility in the data yields $\theta_p = 17$ K. The positive value of θ_p indicates the presence of a strong ferromagnetic exchange interaction in the system. The calculated value of the effective moment (μ_{eff}) is $3.57 \mu_B/\text{Pr}^{3+}$, which is very close to the theoretical value for a free trivalent Pr^{3+} , $g_J[J(J+1)]^{1/2} = 3.58 \mu_B$ for $J = 4$. This result indicates that 4f shell electrons of Pr^{3+} ions are the pre-dominant magnetic species.

Fig. 3 shows the field-dependent isothermal magnetization of $\text{Pr}_2\text{Rh}_2\text{Ga}$ compound. A set of isothermal magnetization $M(H)$ curves were measured with magnetic field as high as 9 T. The measurements were carried out at different temperatures from 2 to 30 K (for both above and below T_C). It is also observed that the magnetization does not reach saturated value even at high field of $H = 9$ T at low temperature of 2 K. The spontaneous magnetization of the compound at 2 K is $1.28 \mu_B/\text{Pr}$. The obtained magnetization of $\text{Pr}_2\text{Rh}_2\text{Ga}$ is smaller than the theoretical value of Pr^{3+} free ions, $g_J = 3.2 \mu_B/\text{Pr}$. The magnetic moment per Pr ions at 9 T for 2 K, is found to be $1.65 \mu_B/\text{Pr}$, which is also two times less than the saturated moment value expected for parallel alignment of free Pr^{3+} . The low saturation value may be attributed to the influence of anisotropy due to the CEF surrounding Pr ions⁶.

3. Heat capacity

Fig. 4a depicts the $C_p(T)$ for $\text{Pr}_2\text{Rh}_2\text{Ga}$ in solid black symbols and non-magnetic reference compound, $\text{La}_2\text{Rh}_2\text{Ga}$ in solid red symbols. At room temperature,

$C_p(T)$ is found to reach a value of 128 J/(mole.K). These values deviate only 3% from the Dulong-Petit value under the formula $C_p = 3nR = 124.7$ J/(mole.K), where n is the number of atoms per formula unit (in this case $n = 5$) and R is the universal gas constant. At low temperatures, $C_p(T)$ shows a λ -type anomaly, which marks the ferromagnetic ordering in the compound. The discontinuous jump with λ -shape anomaly of heat capacity result indicates that the compound undergoes second order ferromagnetic phase transition²⁷.

At low temperature, the heat capacity of the metal is contributed by both electronic and phononic contribution, i.e $C_p = C_{el} + C_{ph}$. The free electron nature of the quasi-particle interactions in an electronic system is indicated by the Sommerfeld coefficient(γ)²⁸. The value of γ can be obtained from the linear fit of the C_p/T vs. T^2 plot by assuming the general expression $C_p = \gamma T + \beta T^3$. In order to perform the fit, the lowest available paramagnetic temperature region was used and is shown in Fig. 4b along with the fitted line (red line). The best fit data yields $\gamma = 640$ mJ/(Pr.mole.K²). The obtained γ value is compared with other heavy fermions Pr-based ternary compounds *viz.*, 286 mJ/(Pr.mole.K²) for PrRhSn₃²⁹, 315 mJ/(Pr.mole.K²) for Pr₂Rh₃Ge⁶, 716 mJ/(Pr.mole.K²) for Pr₃Rh₄Sn₁₃¹, 300 mJ/(Pr.mole.K²) Pr₃Ru₄Ge₁₃³⁰ and 300 mJ/(Pr.mole.K²) for PrV₂Al₂₀⁷. The value obtained here is comparable to the reported value for the Pr-based ternary compounds. The Debye-temperature(θ_D) was also extracted using the fitted value of β and yield $\theta_D = 313$ K.

The inset to Fig. 4a present the low-temperature $C_p(T)$ data in the range between 2 K and 30 K, which were measured under the different values of magnetic field *viz.*, 0, 1 and 5 T. One can see that the peak associated with the phase transition shifts towards higher temperatures with applied magnetic field and also suppresses at high magnetic field of 5 T. This feature is commonly seen in ferromagnetic compounds²⁸. Below T_C , the $C_p(T)$ data can be described with the following formula;

$$C_p(T) = \gamma_e T + BT^{3/2} \exp\left(\frac{-\Delta}{T}\right), \quad (1)$$

where γ_e is the electronic contribution to the heat capacity in the ordered state. The second term $BT^{3/2} \exp\left(\frac{-\Delta}{T}\right)$ represents the spinwave contribution for a ferromagnet with an energy gap $\Delta = E_g/K_B$ in the magnon spectrum of the heat capacity. The best fit on the experimental data is shown in inset of Fig. 4a with solid lines and yielded parameters: $\gamma_e = 0.029(3)$ J/(mole-K²), $B = 0.794(3)$ J/(mole-K²), $\Delta = 8.47(3)$ K in zero field, and $\gamma_e = 0.053(4)$ J/(mole-K²), $B = 0.616(3)$ J/(mole-K²), $\Delta = 7.16(2)$ K in 1 T. The values of Δ are smaller than T_C , which is in good agreement with the previously reported RE₂T₂X system^{31,32}.

The magnetic entropy S_m has been estimated by integrating $(C_m(T)/T)$ as a function of T and is shown in Fig. 4c. Here, $C_m(T)$ was estimated by subtracting of

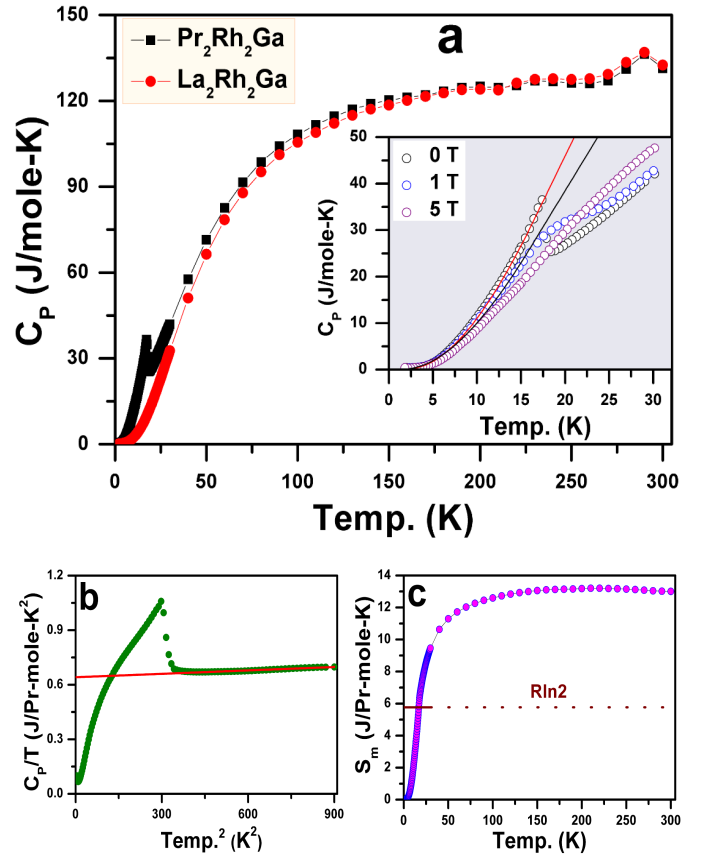


FIG. 4. (a) Temperature dependence of the heat capacity $C_p(T)$ of Pr₂Rh₂Ga measured in zero field. $C_p(T)$ data of the non-magnetic reference compound La₂Rh₂Ga²⁰. Inset: temperature dependent heat capacity under different magnetic field. (b) The low-T part of $C_p(T)/T$ as a function of T^2 together with fitting for evaluating the Sommerfeld coefficient and Debye temperature. (c) The calculated 4f-electron entropy as a function of temperature.

C_p of La₂Rh₂Ga from C_p of Pr₂Rh₂Ga. As seen from Fig. 4c, the S_m released at T_C is very close to the value of $R\ln 2$. This reflects that the Pr has doublet magnetic ground state. It is also noticed that the S_m gradually increases with increasing temperature and fully saturate at 100 K, which is much higher than the phase transition temperature. The obtained saturation S_m value at ≈ 100 K is only about 70 % of the full $R\ln(2J+1)$, $J = 4$ entropy.

4. Electrical resistivity

The $\rho(T)$ of Pr₂Rh₂Ga is presented in Fig. 5. It is observed from Fig. 5 that the resistivity gradually decreases with decreasing temperature and shows well defined kink at the magnetic transition. The compound shows overall metallic behavior. It is also noticed that the resistivity data shows a strong curvature in the paramagnetic region (above 50 K), which is associated with

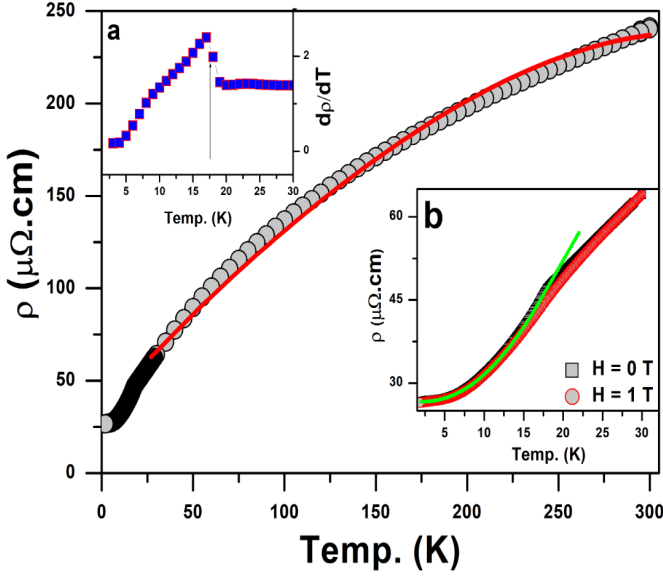


FIG. 5. Temperature dependence of resistivity under zero magnetic field and the red solid line represents the fit of Eq. (2) to the experimental data.. The upper inset (a) $d\rho/dT$ as a function of temperature. The arrow indicates the critical temperature T_C associated with ρ . Inset (b) solid symbols are low-temperature $\rho(T)$ measured under field of 0 and 1 T and the solid line represents the fit of Eq. (3) to the experimental data.

the substantial electron-phonon interaction strength at high temperature and also the scattering effects of the conduction electrons on disordered magnetic moments in combination with the CEF effect⁶. At low temperature, s-d interband scattering of the conduction electrons is related to a Mott term. In the paramagnetic region $T > 50$ K, experimental data of $\rho(T)$ was derived using the following the Bloch - Grüneisen - Mott formula^{33,34}.

$$\rho(T) = \rho_0 + \frac{4A_0}{\theta_R} \left(\frac{T}{\theta_R} \right)^5 \int_0^{\theta_R/T} \frac{x^5 dx}{(e^x - 1)(1 - e^{-x})} - KT^3, \quad (2)$$

where ρ_0 is the residual resistivity typically associated with metallurgical defects. A_0 is the electron-phonon coupling constant. θ_R is the Debye temperature, which represents the characteristic energy scale of lattice vibrations. In the last term, K of Eq.(2) is known as the Mott coefficient, which is a characteristic of s-d interband scattering. The best fits of Eq. (2) with solid line to the experimental $\rho(T)$ vs T data yielded: $\rho_0 = 51.29(2) \mu\Omega.cm$; $\theta_R = 102.84(2) K$; $A_0 = 9.25(4)\mu\Omega.cm.K^{-3}$ and $K = 2.78(3) \times 10^{-6}\mu\Omega.cm.K^{-3}$.

The inset (b) of Fig. 5 depicts an expanded view of $\rho(T)$ data at low temperature. The resistivity decreases sharply below the phase transition which is due to spin disorder scattering of the conduction electrons have been quenched by the magnetic ordering of the spins. The magnetic transition temperature was also evaluated from

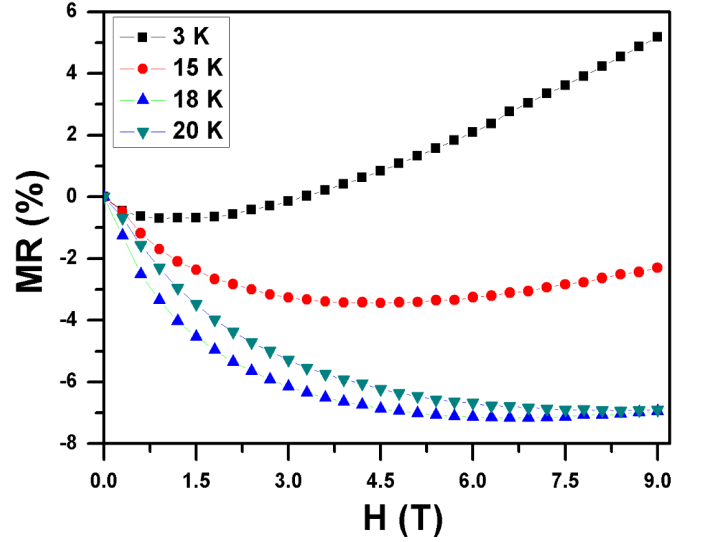


FIG. 6. Field dependence of the magnetoresistance isotherms of $\text{Pr}_2\text{Rh}_2\text{Ga}$ at different temperature near T_C .

$\rho(T)$ result by taking the derivative of ρ with respect to T . The expanded region of $d\rho/dT$ curve at low temperature is presented in inset (a) of Fig. 5. According to Sato criterion³⁵, the value of $T_C = 18$ K was estimated from the midpoint of the anomaly in the $d\rho/dT$ curve, and is marked with an arrow inside of the figure. The magnetic phase transition temperature in ρ is consistent with the results of $\chi(T)$ and $C_p(T)$ data.

In order to analyse the characteristic features for resistivity associated with the magnetic ordered state, the temperature dependence $\rho(T)$ was measured at low temperature under magnetic field value of 1 T and is plotted in the inset (b) of Fig. 5. As seen from the inset (b) of Fig. 5, the anomaly at the transition temperature is suppressed with the application of magnetic field, which is generally seen in a ferromagnetically ordered system. The scattering of the conduction electrons in terms of magnons can be explained through the spin-wave excitation. Below T_C , the temperature variation of ρ under zero-magnetic field data was described by using spin-wave excitation of Eq. (3)³⁶.

$$\rho(T) = \rho_{FM} + A\Delta_R T \left[1 + 2 \frac{T}{\Delta_R} \right] \exp \left[-\frac{\Delta_R}{T} \right], \quad (3)$$

where ρ_{FM} represents the residual resistivity of the magnetic ordered state, A is a material constant which depends on the spinwave stiffness, and Δ_R is associated with the energy gap in the ferromagnetic magnon spectrum. A best fit of Eq.(3) on the experimental result with solid line yields fitting parameters: $\rho_{FM} = 26.6(3) \mu\Omega.cm$, $A = 0.015(2) \mu\Omega.cm.K^{-2}$ and $\Delta_R = 9.01(3) K$.

In order to investigate the magnetoresistance (MR) behavior of $\text{Pr}_2\text{Rh}_2\text{Ga}$, isothermal magnetic field dependence of resistivity was measured at different temperatures for both below and above T_C . MR was calculated

from the isothermal magnetic field dependence of resistivity curve using the following formula of Eq.(4). The obtained MR variation with magnetic field was plotted in Fig. 6.

$$MR = \frac{\rho(H, T) - \rho(0, T)}{\rho(0, T)} 100\% \quad (4)$$

It is seen from Fig. 6 that isothermal MR shows both positive and negative values at high fields of 9 T depending on the temperature. As seen the data for lowest temperature of 2 K, the magnitude of MR is positive above $H = 3$ T and gradually increases with increasing field. However, negative MR is seen for $T = 15$ K and higher. This result indicates that both positive and negative MR can exist below the transition temperature. The negative MR in ferromagnetic region can be attributed to reduction in spin-disorder resistivity. However, the positive MR in ferromagnetic compound can be understood in terms of the Lorentz's force, which causes the classical modification of the electron trajectory⁶. The MR at 20 K just above the T_C shows negative behavior, which may suggest the presence of weak ferromagnetic correlations at 20 K. Similar behavior of MR properties below and above T_C was also reported in the case of $\text{Pr}_2\text{Rh}_3\text{Ge}$ and CeIr_2B_2 compounds^{6,37}.

D. Magnetocaloric effect

The magnetocaloric effect of the $\text{Pr}_2\text{Rh}_2\text{Ga}$ is explored through isothermal magnetization and heat capacity measurements. The order of the phase transition is also confirmed from Arrott plots. Arrott plots (M^2 vs. H/M) were performed from the $M(H)$ curves. Fig. 7 shows the isotherms of M^2 vs. H/M plot in the temperature range of 12 K to 25 K (near the transition temperature region). According to Banerjee criterion, a positive slope in the M^2 vs. H/M plot implies that the system possesses a second order magnetic transition³⁸.

Arrott plots are commonly used to determine the nature of a magnetic phase transition based on the isothermal magnetization data. However, determining the magnetic phase transition from Arrott plot has also some limitation for the shortcomings such as meta-magnetic transition, demagnetization field and domain wall pinning effect³⁹. Therefore, Bonilla and Franco⁴⁰ have suggested one more method to determine the second order of phase transition by employing $-\Delta S_M$ vs. T curve, which will be discussed for this $\text{Pr}_2\text{Rh}_2\text{Ga}$ compound.

The ΔS_M was calculated from isothermal magnetization curve using the following Maxwell relation⁴¹:

$$\Delta S_M(T, H) = \int_0^H \left(\frac{\partial M}{\partial T} \right) dH. \quad (5)$$

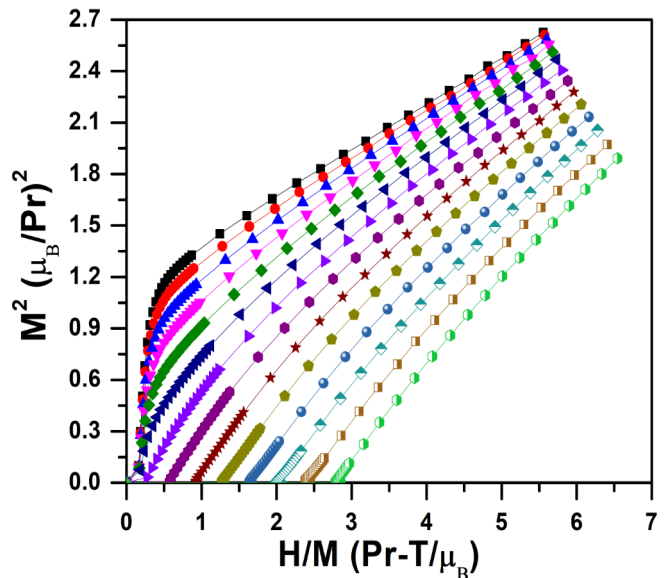


FIG. 7. Arrott plots (M^2 vs. H/M) derived from the magnetization isotherms in the temperature range of 12 - 25 K with a step of 1 K.

Fig. 8 shows the variation of $-\Delta S_M$ as a function of temperature for different values of magnetic field. It is seen that there is no tendency of saturation in $-\Delta S_M$ values even at applied magnetic field strength of 9 T. It is found that the maximum values of $-\Delta S_M$ are 6.1, 7.3 and 8.2 J/kg.K for the change of magnetic field of 0-5 T, 0-7 T, and the 0-9 T, respectively. The obtained $-\Delta S_M$ values are comparable with the reported value of other Pr based ternary compounds *viz.*, $-\Delta S_M = 5.8$ J/kg.K for 7 T of $\text{Pr}_2\text{Pt}_2\text{In}$ and $-\Delta S_M = 6.1$ J/kg.K for 5 T of $\text{Pr}_6\text{Co}_2\text{Si}_3$ ^{31,42}. The observed values are also compared with the some other reported $\text{RE}_2\text{T}_2\text{X}$ compound in Table. II. As seen from the Table. II, the obtained value of $\text{Pr}_2\text{Rh}_2\text{Ga}$ is also quite large and comparable to those of the reported refrigerant materials around corresponding transition temperature. From this comparison, one can say that the present $\text{Pr}_2\text{Rh}_2\text{Ga}$ compound is in a materials class that may profitably be exploited from MCE.

Another important parameter to determine potential of a MCE material is the ΔT_{ad} . The ΔT_{ad} was calculated from temperature dependent zero-field heat capacity data (is shown in Fig. 4) and obtained $-\Delta S_M$, using Maxwell's relation by the following formula⁴¹:

$$\Delta T_{ad} \approx \frac{T}{C_p} |\Delta S_M|. \quad (6)$$

Fig. 9 shows the temperature variation of ΔT_{ad} for the change of magnetic field up to 9 T. The maximum value of ΔT_{ad} was found to be 3.5 K for the change of field 0-9 T. This estimated value of ΔT_{ad} is quite good as compared to some of $\text{RE}_2\text{T}_2\text{X}$ ternary compounds for magneto-refrigerant application¹².

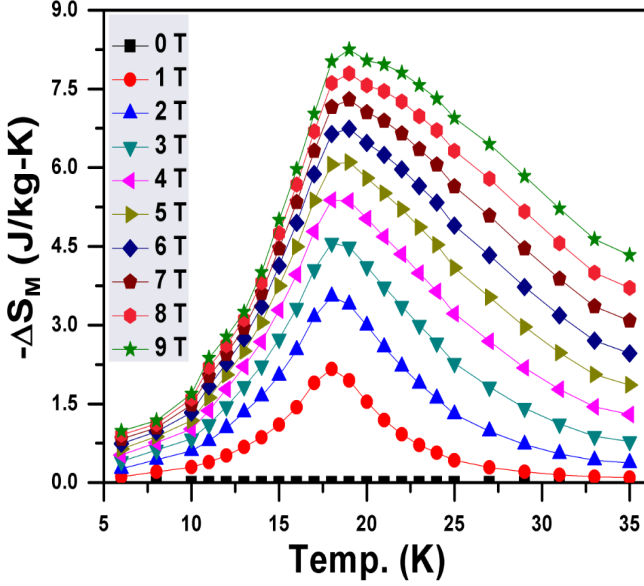


FIG. 8. Temperature variation magnetic entropy changes (ΔS_M) for different values of changing magnetic field

TABLE II. The transition temperature, the maximum values of magnetic entropy change (ΔS_M), and refrigeration capacity (RC) under the field change of 0–5 T for some rare-earth compounds of RE_2T_2X .

Method	T_N/T_C (K)	$-\Delta S_M$ (J/kg.K)	RC (J/kg)	Ref
Nd ₂ Pt ₂ In	16	5.01	—	32
Gd ₂ Ni ₂ Sn	75	4.6	—	43
Er ₂ Co ₂ Al	32	5.9	120	44
Gd ₂ Cu ₂ Cd	120	7.8	234	45
Dy ₂ Co ₂ Ga	55	6.2	114	46
Pr ₂ Rh ₂ Ga	18	6.1	70	This work

Additionally, the quality factor of MCE materials is the refrigeration capacity (RC) which evaluates the magnetic cooling efficiency. RC is an indirect measurement of heat transfer in an ideal MCE cycle between the cold and hot reservoirs. The RC of Pr₂Rh₂Ga was estimated from $-\Delta S_M$ vs. T curve. As suggested by Pecharskya and Gschneidner⁴⁷, the RC value is estimated from the area under the curve by integration using following the formula:

$$RC = \int_{T_1}^{T_2} (-\Delta S_M) dT, \quad (7)$$

where T_1 and T_2 are the temperatures corresponding to both sides of the half-maximum value of the $-\Delta S_M(T)$ peak. It is found that the RC values gradually increase with increasing field. The values of RC are 70 J/kg, 100

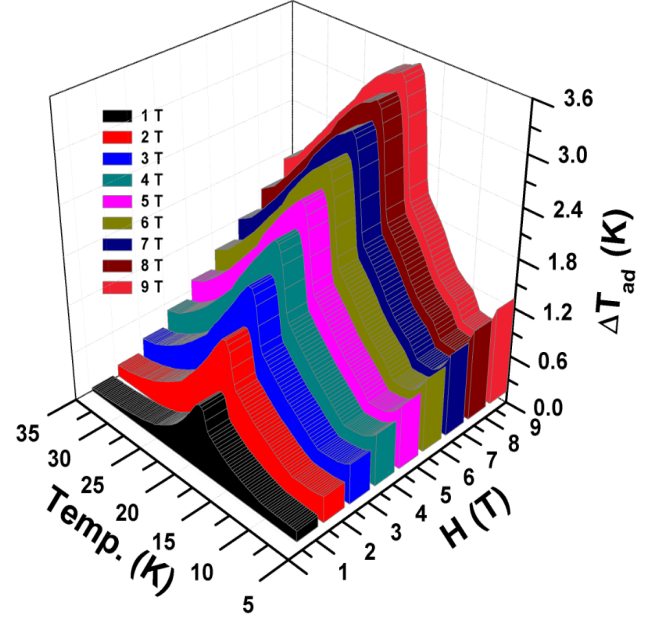


FIG. 9. Temperature variation of the adiabatic temperature change (ΔT_{ad}) for different values of magnetic field.

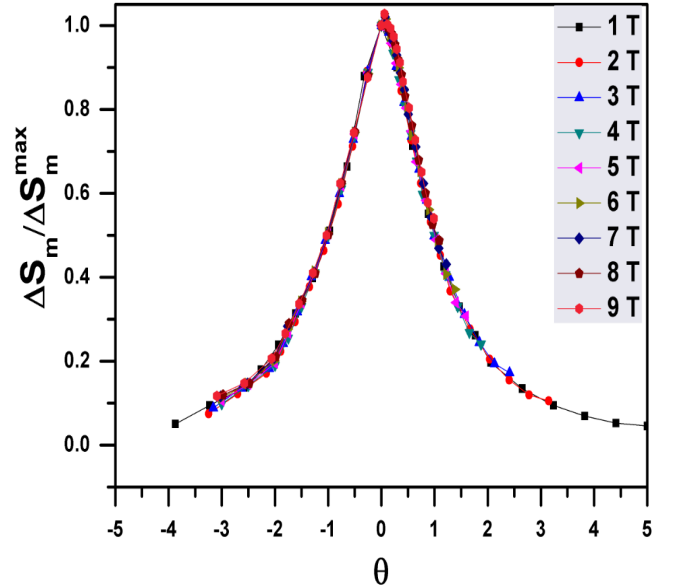


FIG. 10. Normalized entropy change ($\Delta S_M/\Delta S_M^{max}$) as a function of the rescaled temperature(θ) for the selected values of applied field

J/kg and 135 J/kg for a change of field 0–5 T, 0–7 T and 0–9 T respectively. As seen from Table. II, our observed values for the present Pr₂Rh₂Ga compound is comparable even larger than those of some reported magnetic caloric materials

Magnetocaloric effect of a magnetic material also depends on the order of its magnetic phase transition. In order to get more confirmation for the second order mag-

netic phase transition of $\text{Pr}_2\text{Rh}_2\text{Ga}$, we have used universal scaling plots for the magnetic entropy changes⁴⁰. The universal scaling plot is derived from the $-\Delta S_M$ vs. T curve. The normalized entropy change $\Delta S_M/\Delta S_M^{max}$ (where ΔS_M^{max} is the maximum entropy change) against rescaled temperature (θ) for below and above T_C is plotted for different fields and is shown in Fig. 10. The rescaled temperature θ below and above T_C as defined in the following equation

$$\theta = \frac{-(T - T_C)/(T_{r1} - T_C)}{(T - T_C)/(T_{r2} - T_C)}, \quad (8)$$

where T_{r1} and T_{r2} is the temperature corresponding to half of the value of $\Delta S_M/\Delta S_M^{max}$ at $T < T_C$ and $T > T_C$, respectively. As seen from Fig. 10, the normalized entropy change with respect to rescaled temperature converge to a single universal curve for both below and above T_C for different values of magnetic field. This merging to single universal curve indicates that the compound undergo second order ferromagnetic to paramagnetic transition.

E. Summary

In summary, we have successfully synthesized a new polycrystalline compound $\text{Pr}_2\text{Rh}_2\text{Ga}$. This compound crystallizes in the orthorhombic, La_2Ni_3 -type of structure. Magnetic, heat capacity measurements and resistivity results revealed that the present compound undergoes ferromagnetic behavior with the Curie temperature $T_C = 18$ K. We found that $\text{Pr}_2\text{Rh}_2\text{Ga}$ does not have structural phase transition like $\text{Ce}_2\text{Rh}_2\text{Ga}$. The Sommerfeld coefficient value derived from heat capacity shows, a significant enhancement, which gives an indication of a heavy electron ground state in $\text{Pr}_2\text{Rh}_2\text{Ga}$. Resistivity results confirmed that the compound has a metallic-like conductivity character, where the curvature paramagnetic region is observed due to strong electron-phonon scattering. Below T_C , the temperature dependence of heat capacity and resistivity data were well described with the ferromagnetic spin-wave relation. Ferromagnetic spin-wave relation below T_C yields an energy gap value of 8.47(3) K and 9.01(3) K from temperature dependent heat capacity and resistivity data, respectively. This compound exhibits both positive and negative magnetoresistance in the magnetically order state. Arrot plot (H/M vs. M^2) and the universal scaling plot of $-\Delta S_M^{max}$ vs. rescaled temperature (θ) confirm that this compound undergoes a second order paramagnetic to ferromagnetic phase transition. The maximum $-\Delta S_M^{max}$ value of 8.5 J/kg.K and maximum ΔT_{ad} value of 3.6 K are obtained for $\text{Pr}_2\text{Rh}_2\text{Ga}$ under change of field 0–9 T. The corresponding values of RCP is 121 J/kg at 9 T. These obtained values are considerable as compare to the reported MCE materials.

Acknowledgements

This work is supported by Global Excellence and Stature (UJ-GES) fellowship, University of Johannesburg, South Africa. AMS thanks the URC/FRC of UJ for assistance of financial support.

References

- ¹H. S. Nair, O. Michael, S. K. Ghosh, D. T. Adroja, M. M. Koza, T. Guidi, and A. M. Strydom, *J. Phys. Condens. Matter.* **30** (2018) 145601.
- ²T. Ikeno, Y. Isikawa, T. Kuwai, A. Mitsuda, and T. Mizushima, *Physica B: Condensed Matter*, **378** (2006) 677.
- ³P. Fischer, T. Herrmannsdörfer, T. Bonelli, F. Fauth, L. Keller, E. Bauer, and M. Giovannini, *J. Phys. Condens. Matter.* **12** (2000) 7089.
- ⁴M. Giovannini, H. Michor, E. Bauer, G. Hilscher, P. Rogl, and R. Ferro, *J. Alloys. Compd.* **280** (1998) 26.
- ⁵E. A. Goremychkin, R. Osborn, E. D. Bauer, M. B. Maple, N. A. Frederick, W. M. Yuhasz, F. M. Woodward, and J. W. Lynn, *Phys. Rev. Lett.* **93** (2004) 157003.
- ⁶M. Falkowski, and A. M. Strydom, *J. Phys. Condens. Matter.* **29** (2017) 395601.
- ⁷A. Sakai, and S. Nakatsuji, *J. Phys. Soc. Jpn.* **80** (2011) 063701.
- ⁸E. D. Bauer, N. A. Frederick, P.-C. Ho, V. S. Zapf, and M. B. Maple, *Phys. Rev. B* **65** (2002) 100506.
- ⁹J. L. Zhang, Y. Chen, L. Jiao, R. Gumenuk, M. Nicklas, Y. H. Chen, L. Yang, B. H. Fu, W. Schnelle, H. Rosner, A. Leithe-Jasper, Y. Grin, F. Steglich, and H. Q. Yuan, *Phys. Rev. B* **87** (2013) 064502.
- ¹⁰F. Morales, R. Escudero and A. Durán, *J. Low Temp. Phys.* **153** (2008) 15.
- ¹¹V. N. Narozhnyi, J. Freudenberger, G. Fuchs, K. A. Nenkov, D. Eckert, A. Czopnik A and K. H. Müller *J. Low Temp. Phys.* **117** (1999) 1599.
- ¹²Y. Zhang, *J. Alloys Compd.* **787** (2019) 1173-1186.
- ¹³L. Mařyana, and R. Pöttgen, *Z. Kristallogr. Cryst. Mater.* **218** (2003) 767–787.
- ¹⁴K. A. Gschneidner, J.C. Bünzli and V.K. Pecharsky, "Handbook on the physics and chemistry of rare earths" Newnes. (2004) 13.
- ¹⁵M. S. Kim, M. C. Bennett, and M. C. Aronson, *Phys. Rev. B* **77** (2008) 144425.
- ¹⁶I. R Fisher, Z. Islam, and P. C. Canfield, *J. Magn. Magn. Mater.* **202** (1999) 1.
- ¹⁷B. Heying, U. C. Rodewald, and B. Chevalier, *Zeitschrift für Naturforschung B* **68** (2013) 10.
- ¹⁸M. Pani, F. Merlo, and M. L. Fornasini, *Zeitschrift für Kristallographie-Crystalline Materials* **217** (2002) 415.
- ¹⁹V. A. Romaka, Y. Grin, Y. P. Yarmolyuk, O. S. Zarechnyuk, R. V. Skolozdra, *Physics of Metals and Metallography* (translated from *Fizika Metallov i Metallovedenie*) **54** (1982) 58-64.
- ²⁰A. Strydom, A. Tursina, S. Nesterenko, and M. Baenitz, to be published.
- ²¹Rietveld H. M., *Journal of Applied Crystallography*, **2** (1969) 65.
- ²²J. Rodriguez-Carvajal, Fullprof Suite <http://www.ill.eu/sites/fullprof/> (2017).
- ²³J. H. N. Van Vucht, and K. H. J. Buschow, *J. Less. Common. Met.* **46** (1976) 133.
- ²⁴F. Izumi and K. Momma, *Proc. XX Conf. Appl. Crystallogr., Solid State Phenom.* **130** (2007) 15-20.
- ²⁵E. Teatum, K. Gschneidner, J. Waber, *Compilation of calculated data useful in predicting metallurgical behavior of the elements in binary alloy systems*, LA-2345, Los Alamos Scientific Laboratory (1960).

- ²⁶A. H. Morrish, *The Physical Principles of Magnetism* (Warszawa: PWN) (1970).
- ²⁷S. Pakhira, C. Mazumdar, R. Ranganathan, S. Giri, and M. Avdeev, *Phys. Rev. B* **94** (2016) 104414.
- ²⁸A. Tari, *The Specific Heat of Matter at Low Temperatures* (London: Imperial College Press) (2003).
- ²⁹V. K. Anand, D. T. Adroja and A. D. Hillier, *Phys. Rev. B* **85** (2012) 014418.
- ³⁰S. Ramakrishnan, K. Ghosh, S. K. Dhar, S. K. Malik, G. Chandra and R. Vijayaraghavan, *J. Magn. Magn. Mater.* **152** (1996) 375.
- ³¹J. J. Mboukam, B. M. Sondezi, M. B. T. Tchokonté, A. K. H. Bashir, A. M. Strydom, D. Britz, and D. Kaczorowski, *Physica B: Condensed Matter.* **536** (2018) 505.
- ³²M. B. T. Tchokonté, J. J. Mboukam, A. K. H. Bashir, B. M. Sondezi, K. Ramesh Kumar, A. M. Strydom, and D. Kaczorowski, *J. Alloys. Compd.* **753** (2018) 41.
- ³³N. F. Mott, H. Jones, *The Theory of the Properties of Metals and Alloys*, Oxford University Press, London (1958).
- ³⁴G. Grimvall, *The Electron - Phonon Interaction in Metals*, North - Holland, Amsterdam (1981).
- ³⁵N. Sato, N. Aso, K. Hirota, T. Komatsubara, Y. Endoh, S.M. Shapiro, G.H. Lander, K. Kakurai, *Phys. Rev. B* **53** (1996) 14043.
- ³⁶M. B. Fontes, J. C. Trochez, B. Giordanengo, S. L. Bud'ko, D. R. Sanchez, E. M. Baggio-Saitovich, and M. A. Continentino, *Phys. Rev. B* **60** (1999) 6781.
- ³⁷A. Prasad, V. K. Anand, U. B. Paramanik, Z. Hossain, R. Sarkar, N. Oeschler, M. Baenitz and C. Geibel *Phys. Rev. B* **86** (2012) 014414.
- ³⁸S.K. Banerjee, *Phys. Lett.* **12** (1964) 16.
- ³⁹K. K. Ramesh, H. S. Nair, A. Bhattacharyya, A. Thamizhavel, and A. M. Strydom. *J. Magn. Magn. Mater.* **452** (2018) 205–209.
- ⁴⁰C. M. Bonilla, J. Herrero-Albillos, F. Bartolomé, L. M. García, M. Parra-Borderías, and V. Franco, *Phys. Rev. B* **81** (2010) 224424.
- ⁴¹A. M. Tishin and Y. I. Spichkin, *The Magnetocaloric Effect and Its Applications* (IOP, New York, 2003).
- ⁴²A.K. Pathak, I. Dubenko, S. Stadler, N. Ali, *J. Appl. Phys.* **109** (2011) 07A913.
- ⁴³P. Kumar, N. K. Singh, K. G. Suresh, and A. K. Nigam, *Phys. Rev. B* **77** (2008) 184411.
- ⁴⁴X. Dong, J. Feng, Y. Yi, and L. Li, *J. Appl. Phys.* **124** (2018) 093901.
- ⁴⁵Y. Yang, Y. Zhang, X. Xu, S. Geng, L. Hou, X. Li, Z. Ren, and G. Wilde, *J. Alloys Compd.* **692** (2017) 665–669.
- ⁴⁶Y. Zhang, D. Guo, S. Geng, X. Lu, and G. Wilde, *J. Appl. Phys.* **124** (2018) 043903.
- ⁴⁷V. K. Pecharskya and K. A. Gschneidner Jr., *J. Appl. Phys.* **90** (2001) 4614.